Journal of Materials Chemistry B

Accelerated Dermal Wound Healing in Diabetic Mice by H_2O_2-Generating Catechol-Functionalized Gelatin Microgel

Journal:	*Journal of Materials Chemistry B*
Manuscript ID	TB-ART-08-2024-001722.R1
Article Type:	Paper
Date Submitted by the Author:	19-Jan-2025
Complete List of Authors:	Forooshani, Pegah; Michigan Technological University, Biomedical Engineering Razaviamri, Fatemeh; Michigan Technological University, Biomedical Engineering Smies, Arian; Michigan Technological University, Biomedical Engineering Morath, Lea; Michigan Technological University, Biomedical Engineering Pinnaratip, Rattapol; Michigan Technological University, Biomedical Engineering Bhuiyan, Md. Saleh Akram ; Michigan Technological University, Biomedical Engineering Rajachar, Rupak; Michigan Technological University, Biomedical Engineering Goldman, Jeremy; Michigan Technological University, Biomedical Engineering Lee, Bruce; Michigan Technological University, Biomedical Engineering

ARTICLE

Accelerated Dermal Wound Healing in Diabetic Mice by H_2O_2-Generating Catechol-Functionalized Gelatin Microgel

Received 00th January 20xx,
Accepted 00th January 20xx

DOI: 10.1039/x0xx00000x

Pegah Kord Forooshani, Fatemeh Razaviamri, Ariana Smies, Lea M. Morath, Rattapol Pinnaratip, Md Saleh Akram Bhuiyan, Rupak Rajachar, Jeremy Goldman, Bruce P. Lee *

Physically crosslinked gelatin microgels were functionalized with a bioadhesive molecule, catechol, to study the effect of in-situ generated H_2O_2 on full-thickness wound repair in diabetic mice. Due to the physically crosslinked nature of the microgels, they transition into a hydrogel film upon hydration. The formation of hydrogel film was confirmed by the changes in its morphology and viscoelastic properties. Additionally, these microgels released up to 86 μM of H_2O_2 as a result of catechol autoxidation. The generated H_2O_2 completely eradicated *Staphylococcus epidermidis* with an initial concentration of 10^3 CFU/mL. These microgels were not cytotoxic and promoted VEGF upregulation in immortalized human keratinocytes (HaCaT) in-vitro. When the microgels were applied to full-thickness dermal wound in diabetic mice, dermal wound closure was accelerated over 14 days, achieving a wound closure of 90% based on the wound area. Microgel-treated wounds also resulted in complete re-epithelialization and regeneration of new dermal tissues with morphology and structure resembling native tissues. These results indicate that the release of micromolar concentrations of H_2O_2 can accelerate wound healing in healing-impaired animal.

1. Introduction

Diabetes mellitus (DM) is one of the most prevalent and challenging diseases with around 425 million patients reported in 2017 worldwide and the number is predicted to grow each year [1]. Among patients living with DM, 25% will develop a foot ulcer. Just in the US alone, more than 1 million cases of diabetic foot ulcer complications were reported from 2006 to 2010 [2]. Diabetic ulcers may take over 3 months to heal and are more susceptible to infection, which can result in undesirable clinical outcomes, including sepsis, amputation, and death [3, 4]. Current treatments include local delivery of growth factors, bioengineered skin grafts, and negative wound therapy, which are costly and have demonstrated mixed results [5, 6]. Most importantly, these treatments do not actively prevent infection.

Rapid dermal healing requires a balance of redox control [7, 8]. During the early phases of wound healing, neutrophils and macrophages are attracted to the wound site and release reactive oxygen species (ROS), such as hydrogen peroxide (H_2O_2) at concentrations in the micromolar range. H_2O_2 induces vascular endothelial growth factor (VEGF) expression in keratinocytes [9], which stimulates angiogenesis in wounds [10]. ROS is also necessary in the differentiation of M2 macrophage [11], which promotes tissue regeneration and anti-inflammatory responses [12, 13]. Application of ROS to chronic ulcers (e.g., direct application of H_2O_2, hyperbaric treatment to enhance ROS concentration, application of honey, etc.) has been found to accelerate healing [8, 14]. Additionally, ROS provides a natural defense against bacterial infection [15]. However, high levels of ROS can destroy healthy tissues, resulting in the formation of chronic wounds and promote tumor initiation [16, 17]. Biomaterials supplemented with antioxidants have been found to accelerate wound healing, reduce chronic inflammation, and increase biocompatibility [18, 19]. However, complete removal of ROS delayed wound healing [8]. Thus, H_2O_2 concentration needs to be carefully tuned to achieve rapid dermal wound healing.

Catechol is an adhesive moiety found in mussel adhesive proteins and imparts these proteins with strong, moisture-resistant adhesive properties [20, 21]. During the oxidation of catechol, ROS, such as superoxide anion ($O_2^{\cdot -}$) and H_2O_2, are generated as byproducts [22-24]. Previously, our lab employed this unique redox chemistry to create biomaterials that can be activated to generate H_2O_2 through simple hydration [25-29]. Molecular oxygen found in the aqueous solution initiates catechol autoxidation and H_2O_2 generation. The generated H_2O_2 effectively disinfected both gram-negative and positive bacteria as well as both enveloped and non-enveloped viruses [25, 27, 29]. Recently, catechol-generated H_2O_2 was demonstrated to accelerate dermal wound healing in wild type mice with normal wound healing behaviors [30]. However, the effect of catechol-generated H_2O_2 on healing-impaired wounds has not been previously demonstrated.

Depart of Biomedical Engineering, Michigan Technological University, Houghton, Michigan 49931.

† Footnotes relating to the title and/or authors should appear here.

Electronic Supplementary Information (ESI) available: [details of any supplementary information available should be included here]. See DOI: 10.1039/x0xx00000x

Here, we developed a catechol-modified microgel system to study the effect of the generated H_2O_2 on the healing of full-thickness dermal wounds in a diabetic mice model (**Figure 1**). The diabetic mice model is one of the most suitable models for studying delayed wound healing, where wound closure is delayed by 7-10 days, regardless of the wound size, when compared to that of healthy mice [31]. Physically crosslinked gelatin microgels were functionalized with catechol moieties that can generate H_2O_2 when hydrated in an aqueous solution. Gelatin is a water-soluble protein extracted from collagen and is known for its excellent biocompatibility, biodegradability, and low cost [32-34]. Gelatin has been extensively studied as a biomaterial for different biomedical applications, including drug delivery, tissue engineering, and biological glues, as it promotes cell adhesion, migration, and proliferation [33-36]. Most importantly, gelatin retains the ability to self-assemble into a hydrogel network through physical interactions such as hydrogen bonds and Van der Waals forces [37]. We envision that the physically crosslinked microgels can undergo a physical transition to form a hydrogel film when hydrated in an aqueous solution. Additionally, the presence of catechol will function as a source for H_2O_2 generation to improve dermal wound healing and function as a disinfectant.

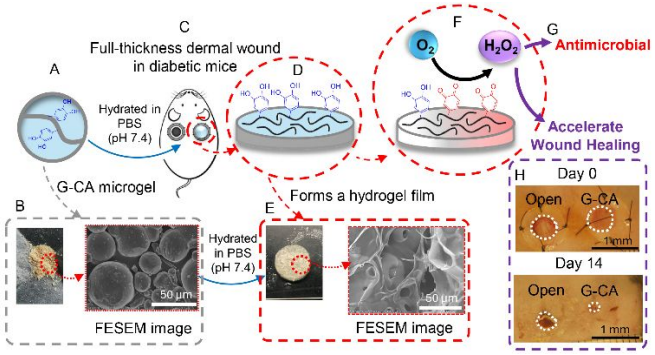

Figure 1. (A) Schematic representation and (B) images of catechol-modified microgels (G-CA) and (C) its application to full-thickness dermal wounds created in a healing-impaired diabetic mouse model. (D, E) Hydration of microgels results in their physical transition to form a wound-covering hydrogel film. (F) Catechol autoxidation generates H_2O_2 as a byproduct, which (G) functions as a disinfectant, and (H) can promote wound healing in diabetic mice.

In this study, physically crosslinked gelatin microgels were functionalized with various amounts of 3,4-dihydroxyphenylacetic acid (DOPAC), which contains a catechol side chain (**Figure 2**). The transition of these microgels to hydrogel films were characterized based on the changes to their morphology and viscoelastic behaviors using scanning electron microscopy (SEM) imaging and oscillatory rheometry, respectively. The ability for the microgel to generate H_2O_2 when hydrated was investigated. Additionally, the ability for the generated H_2O_2 to kill gram-positive bacteria, *Staphylococcus epidermidis*, and accelerate wound healing in a full-thickness dermal wound model using healing-impaired diabetic mice were investigated.

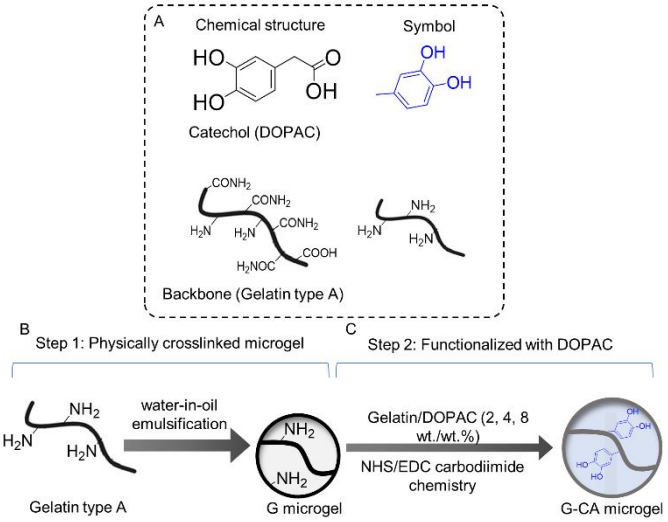

Figure 2. (A) Chemical structure of DOPAC and schematic representation of gelatin. 2-step preparation process involving (B) the preparation of physically crosslinked gelatin microgels in a water-in-oil emulsion followed by (C) functionalizing the microgel with DOPAC through carbodiimide chemistry.

2. Materials and Methods

2.1. Material

Gelatin powder (type A, 300 Bloom, from porcine skin) was purchased from Electron Microscopy Sciences. DOPAC, 1-ethyl-3-[3-dimethylaminopropyl]carbodiimide hydrochloride (EDC), *N*-hydroxysuccinimide (NHS), phosphate-buffered saline (PBS, BioPerformance certified, pH 7.4), (3-aminopropyl) triethoxysilane (APTS), histology mounting medium Polyfreeze, Trichrome Stain (Masson) Kit, Bouin's solution, Weigert's iron hematoxylin solution, and TWEEN 80 were purchased from Sigma-Aldrich (St. Louis, MO). Pierce Quantitative Peroxide Assay Kit with sorbitol was obtained from Thermo Scientific (Rockford, IL). Tryptic soy broth (TSB), Mueller Hinton agars (28 mL fill, 15 × 100 mm), and astral inoculation loop (10 µL, sterilized) were obtained from Hardy Diagnostics (Santa Maria, CA). *S. epidermidis* (ATCC 12228) were obtained from American Type Culture Collection (ATCC, Manassas, Virginia). Anprolene gas sterilization and gas refills (ethylene oxide) were obtained from Andersen Sterilizers, Inc. (Haw River, NC). Dulbecco's Eagle's Minimum Essential Media (DMEM) and Biotium Resazurin Cell Viability Assay Kit (2500 assays) were purchased from Thermo Fisher Scientific (Rockford, Illinois). Human vascular endothelial growth factor (VEGF) Quantikine ELISA Kit (Catalog #DVE00) was purchased from Bio-Techne (Minneapolis, MN). Goat anti-rabbit IgG H&L (Alexa Fluor 488) (ab150077), anti-CD68 antibody (ab125212), and goat anti-rabbit IgG H&L (Alexa Fluor 647) were purchased from Abcam (Cambridge, MA). 4,6-Diamidino-2-phenylindole (DAPI) was obtained from Invitrogen (Grand Island, NY). Nylon Suture 5-0

(1X18" C-3) was purchased from Ethicon. C57BLKS/J-m+/+Lepr db mice were purchased from Jackson Laboratory (Bar Harbor, ME). All animal work was approved by the Michigan Technological University Institutional Animal Care and Use Committee (IACUC protocol number 828996-9).

2.2. Preparation of Microgels

Microgels were prepared in two steps (**Figure 2**). During the first step, physically crosslinked gelatin microgels (G) were prepared through a water-in-oil emulsification approach following a previously published protocol [36]. 2.5 g of gelatin powder was dissolved in 25 mL of deionized (DI) water by stirring in a heated water bath (50–55 °C). The gelatin solution was then transferred drop by drop to 250 mL of preheated olive oil (50–55 °C) and stirred at 1000 rpm using an overhead mechanical stirrer for 1 h. Then, the emulsion was cooled down in succession by keeping it at room temperature for 30 min followed by submersion in an ice-water bath for an additional 30 min while stirring at the same speed. 150 mL of pre-cooled acetone (4 °C) was further added into the mixture while stirring for another 30 min in the ice-water bath. Microgels were collected using filter paper, washed twice with pre-cooled acetone, and dried under vacuum overnight.

In the second step, G was further functionalized with DOPAC through carbodiimide chemistry. Different amounts of DOPAC (DOPAC/G= 2, 4, 8 wt/wt%), NHS, and EDC (NHS:EDC:DOPAC = 1:4:1 molar ratio) were dissolved in 30 mL of PBS (pH=5.7) that contains 0.5% TWEEN 80 and stirred for 15 min at 25 °C. 500 mg of G was added to the reaction mixture to form a suspension and shaken using an orbital shaker at 4 °C for 24 h. Finally, microgels were collected by centrifugation at 5000 rpm for 5 min and washed twice with pre-cooled (4 °C) acetone. The collected microgels were lyophilized for 24 h to yield a dried powder. The microgels were denoted as G-2CA, G-4CA, and G-8CA based on the DOPAC content.

2.3. Formation of Hydrogel Film

The dried microgels (15 mg) were hydrated with 225 µL of PBS (pH 7.4) and lightly shaped in between two glass slides using a silicone rubber ring as a mold (diameter 10 mm, thickness = 0.85 mm, **Figure S1A**). After removing the mold, the shaped microgels were incubated for 24 h at 37 °C to form a film (**Figure S1B**).

2.4. Characterization of Microgels

Microgels were characterized using attenuated total reflectance Fourier-transform infrared (ATR–FTIR) spectroscopy (Shimadzu IRTracer-100) with a scan rate of 800 scans per minute at the resolution of 1 cm^{-1}. The concentration of DOPAC in the microgels network was determined using UV–vis (PerkinElmer Lambda35). The microgels (10 mg) were solubilized in 5 ml acidic DI water (pH 3.5) by stirring with a magnetic stir bar for 2 h in a heated water bath (50–55 °C). The microgels were condensed by centrifugation at 5000 rpm for 5 min, and the concentration of the DOPAC in the supernatant solution was determined using the UV–vis at the wavelength of 280 nm. The experiment was conducted in triplet and the results are reported as mean ± standard deviation (SD).

2.5. H_2O_2 Concentration Determination

The microgels (10 mg) were hydrated in 300 µL of PBS (pH 7.4) and incubated for up to 24 h at 37 °C with gentle agitation on a shaking plate. A Quantitative Peroxide Assay Kit (i.e., ferrous oxidation–xylenol orange assay) was used to quantify the H_2O_2 concentration following the published protocol [38]. A series of solutions containing 0–1 mM of H_2O_2 were used to prepare a standard curve. The experiment was conducted in triplet and the results are reported as mean ± SD.

2.6. Field Emission Scanning Electron Microscopy (FESEM)

Morphologies of dried microgels and hydrogel films were determined using FESEM (Hitachi S-4700). The hydrogel films were prepared as described above and then lyophilized before imaging. Samples were coated with a 2 nm thick Pt/Pd coating and characterized using FESEM.

2.7. Oscillatory Rheometry

Rheological properties of microgel suspension and the resulting film were characterized using a HR-2 rheometer (TA Instruments, New Castile, DE, USA). A strain sweep experiment (0.001 - 5% strain at 0.1 Hz) was performed to determine the storage (G') and loss (G") moduli. 15 mg of microgels were hydrated with 225 µL of PBS (pH 7.4) in a silicone rubber mold. For the microgel suspension, the samples were formed directly on the rheometer and tested immediately after hydrating the microgels. For the film, samples were tested after the samples were incubated at 37°C for 48 h. Samples were tested using a parallel plate setup (diameter 20 mm) at a gap distance that is set at 90 % that of the individual hydrogel thickness, as measured by a digital calliper.

2.8. Johnson-Kendall-Robert (JKR) Contact Mechanics Test

The adhesive property of the hydrogel films were measured using the JKR contact mechanics test following published protocol [39]. A quartz hemisphere was first functionalized with amine end groups through silane chemistry to mimic the functional groups that exist on the skin tissue, following a previously published protocol [40, 41]. Briefly, the quartz hemispheres were first sonicated in acetone for 15 min, immersed into 3 v/v % APTS solution in acetone for 5 min, and sonicated for 15 min. Finally, they were soaked in acetone for 10 min, dried at room temperature, and baked overnight at 60 °C.

The amine-functionalized quartz hemisphere was attached to the indenter and compressed on a hydrogel film with a speed of 1 µm/s until a maximum compressive force of 10 mN was achieved. After 1 min, the indenter was retracted at the same speed while measuring the tensile force. The force (F) vs.

displacement (δ) curve obtained from JKR contact mechanics tests was integrated to obtain work of adhesion (W_{adh}) according to the equation below [42]:

$$W_{adh} = \int \frac{F\, d\delta}{A_{max}} \quad (1)$$

where A_{max} is the maximum area of contact between the indenting surface and the sample. A_{max} was determined from fitting the loading portion of the JKR contact curve with Hertzian model [43] following a published protocol [44]. The experiment was conducted in a triplet, and the results are reported as mean ± SD.

2.9. Antibacterial Properties

The antibacterial activities of the microgels were evaluated using *S. epidermidis* while following published protocol with some modifications [45]. *S. epidermidis* grown on agar plates was diluted by a sterile solution of 5 v/v% broth in PBS to 10^3 CFU/mL. The ethylene oxide-sterilized microgels (33 mg) were equilibrated with 300 µL of sterile PBS (pH 7.4) and 700 µL of bacteria suspension was added. The microgel and bacteria mixture was incubated at 37 °C for 24 h with gentle agitation on a shaking plate (130 rpm). At a given time point (3, 6, and 24 h), a 10 µL loop was immersed into the mixture and streaked onto agar plates, which were further incubated at 37 °C for 48 h. The agar plates with colonies were photographed, and the bacteria colonies were counted using ImageJ. The Log reduction values (LRV) were calculated following the equation below [46]:

$$LRV = Log_{10}\left(\frac{A}{B}\right) (2)$$

where A is the colony numbers formed from the bacteria cultured in 5 v/v% broth that did not contain any microgel (control) and B is the number of colonies formed from the bacteria exposed to microgels. The experiment was performed in triplet, and the results are reported as mean ± SD.

2.10. Cell culture

Immortalized human keratinocyte line HaCaT [47] were cultured in DMEM Medium), supplemented with 10% fetal bovine serum (FBS), 100 U/mL penicillin, and 100 µg/mL streptomycin. Cells were incubated at 37°C with 5% CO_2 for until they reached confluency and were ready to be passaged for the cytotoxicity and ELISA assays.

2.11. Cytotoxicity

To assess the cytotoxicity of the microgels, 96-well plates were coated with 100 µL microgel suspension (10% in DMSO) and dried under vacuum conditions overnight. The well plates were sterilized using UV irradiation for 30 min. After sterilization, HaCaT cell solutions with and without catalase (2000-5000 U/mL) were added to the well plates at a density of 20,000 cells/cm^2 and incubated for 48 h. Cell viability was assessed using the resazurin assay following a published protocol [48]. The results were normalized based on the cell viability for cells seeded in polystyrene tissue culture wells. Five replications were performed per treatment, and results were reported as mean ± standard deviation (SD).

2.12. Enzyme-linked immunosorbent (ELISA) assay

VEGF levels in the culture supernates of HaCaT cells were measured using the Human VEGF Quantikine ELISA Kit according to the manufacturer's protocol with minor modifications. HaCaT cells were seeded in 48-well plates at a density of 20,000 cell/cm^2 and treated with 10 mg of microgels for 24 hours at 37°C and 5% CO_2, while untreated cells cultured on polystyrene (PS) served as the control.

Culture medium was centrifuged at 1000× g for 10 minutes to remove cellular debris. 200 µL of the collected supernate was added into duplicate wells of the 96-well plates of the ELISA kit, and a standard curve was prepared by serial dilution of the known standards (range: 0–1000 pg/mL, **Figure S2**). Absorbance was measured at 450 nm, with a reference wavelength of 540 nm, using a microplate reader. VEGF concentrations were calculated by superimposing the absorbance values onto the prepared standard curve. All experiments were performed in triplicate, and results were reported as mean ± standard deviation (SD).

2.13. Full-Thickness Dermal Wound Healing Model

Female C57BLKS/J-m+/+Lepr ^{db} mice (diabetic mice, 10-weeks old, weight 40 g, Jackson Laboratory) were used to study full-thickness dermal wound healing. The experiment was performed following published protocol with some modifications [49-51]. Mice were anesthetized (using 3% isoflurane in oxygen when in chamber and then 2 % isoflurane with 1.5 L oxygen when using a nose cone) and the hair was removed before wounding [52]. Two full-thickness excision wounds were

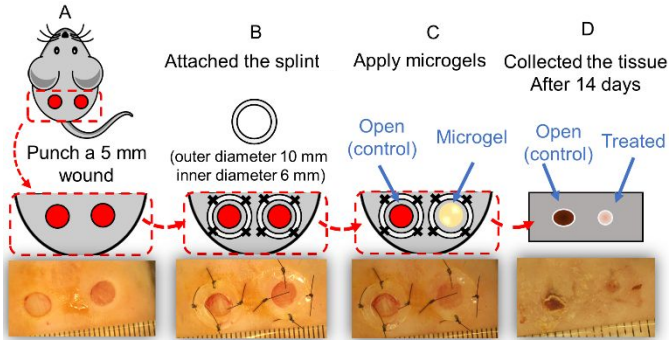

Figure 3. Schematic representations and photographs of the step-by-step process for creating and treating the full-thickness wound model in C57BLKS/J-m+/+Lepr ^{db} mice. (A) Two full-thickness excision wounds were created with a 5-mm dermal punch. (B) The wounds were splinted to avoid skin contraction by fixing a silicone ring to the skin using an adhesive and sutures. (C) The wounds were either left open or treated with microgels. (D) The tissue surrounding the wound was removed for histological analysis.

created with a 5-mm dermal punch on the dorsal skin of the mice (**Figure 3A**). The size of the wounds was fixed using a transparent medical-grade silicone ring (outer diameter 10 mm, inner diameter 6 mm) as a splint to reduce the contraction of the wounds (**Figure 3B**). Fixing the wound with silicon splints is critical to prevent skin contraction and create a model which mimics human-like wound healing [49-51]. The ring was glued to the skin using cyanoacrylate glue and stitched with a 5-0 nylon suture. The wounds were either treated with one of the microgels (treatments) or left open (OP, control) (**Figure 3C**). Microgels (10 mg) were equilibrated with 100 µL sterile PBS (pH 7.4) before administration. The wounds were covered with a non-adhering dressing mesh designed to minimize wound adherence. The wounds were finally sealed off using a sticky adhesive film. Wound dressings were replaced every day for the first three days post-surgery, and a pain killer was administered (20 µL/12 h). The size of the wounds was monitored and photographed on days 0 and 14. The animals were euthanized on day 14, and the tissue surrounding the wound was removed for histological analysis (**Figure 3D**). The number of repeats per test group at each time point was three.

2.14. Analysis of Wound Closure

Wound closure was evaluated on days 0 and 14. An image was taken from each wound while a ruler was placed alongside the wound. The area of each wound was measured using ImageJ, and the percentage of wound closure was calculated following the equation below [53]:

$$Wound\ closure\ \% = \frac{A - B}{A} \times 100\% (3)$$

where, A is the area of the wound on day 0, and B is the area of the wound on day 14.

2.15. Immunological and Histological Analysis

After harvesting the dorsal tissue on days 7 and 14, they were immersed in Polyfreeze and flash-frozen in a liquid nitrogen bath and stored at -80 °C. The samples were sectioned to create 10-µm thick sections and mounted onto a glass slide. The histological analysis of the dermal wounds was performed by trichrome staining to evaluate cellular infiltration, epidermis analysis, and collagen deposition, following a published protocol with minor modifications [54].

Tissue samples were obtained from the -80 °C freezer, incubated in a preheated Bouins' solution (56 °C) for 15 min, and rinsed in running tap water until it was clear. Then, tissue samples were incubated in the hematoxylin stain for 5 min before being washed under running tap water for an additional 5 min. Tissue samples were further incubated in a scarlet red solution for 5 min and rinsed in a DI H_2O bath. A solution of phosphomolybdic, phosphotungstic acid and DI H_2O in 1:1:2 volume ratio was applied on the top of the tissue and incubated for 5 min. Finally, a methylene blue solution was added and incubated for 3 min before being washed using 1% acetic acid. Samples were dehydrated and cleared in xylene and then mounted using a permanent mounting medium.

The population of keratinocytes was examined using keratin-6 (K-6) staining to analyze the wound maturity using a previously established protocol with minor modifications [55]. Briefly, tissue samples were incubated in a blocking solution (3% normal goat serum [NGS]) for an hour and then incubated in a K-6 antibody (1:2000 dilution in NGS) overnight at -4 °C. They were then washed in PBS and incubated for an additional hour in a biotinylated antibody (1:4000 dilution). The tissue samples were washed again to remove the extra antibody. Vectastain ABC-kit was used to complete the staining. Finally, the tissue samples were incubated with the DAB solution until the desired color intensity was observed and further counterstained using toluidine blue.

The tissue samples were imaged using an EVOS microscope. The overlapped images were processed via the Adobe Photoshop program auto stitching module. All images were measured and analyzed by ImageJ [56]. Collagen layer thickness (%) and K-6 positive cell (%) were determined by measuring the blue and brown color in a 1 mm × 1 mm box selected on the wound bed, respectively, using ImageJ.

Macrophage populations were evaluated using CD68-DAPI fluorescence staining, following a published protocol with some modifications [54]. Tissue samples were fixed in 100% ethanol for 5 min and dipped in a PBS bath for an additional 5 min. A hydrophobic marker was used to draw a circle around each tissue section. 10% Goat Serum (diluted in PBS) was applied and incubated for 30 min. After washing with PBS, the tissue samples were incubated with 1 drop of biotin and 1 drop of avidin solutions for 10 min. Samples were washed twice with PBS and incubated in a 1:100 dilution of primary anti-CD68 for 1 h. The samples were incubated in a 1:200 dilution of secondary antibody for 1 h after being washed twice with PBS. Samples were washed again in PBS and incubated in a 1:500 dilution of streptavidin for 1 h (preserved from light). The samples were then stained by 1:1000 dilution of DAPI for 2 min and mounted using an aqueous mounting medium. The image of the tissue samples was taken immediately after the staining. Inflammatory response was evaluated by determining the total number of CD68-stained macrophages to the total number of DAPI-stained cells in three randomly selected 0.5 mm × 0.5 mm boxes on the wound bed using ImageJ.

2.16. Statistical Analysis

Statistical analyses were performed using SigmaPlot. One-way analysis of variance (ANOVA) with Tukey method was used for comparing means of multiple groups.

3. Results and Discussions

3.1. Microgel Preparation and Characterization

Catechol-containing microgels were prepared by functionalizing physically crosslinked gelatin microgels with DOPAC through carbodiimide chemistry. DOPAC contains a catechol moiety that can function both as a bioadhesive molecule and a source for H_2O_2 generation. ATR–FTIR spectra of catechol-containing microgels exhibited the characteristic peaks for catechol at 868 and 922 cm^{-1}, which is associated with the out-of-plane bending of =C-H bonds of an aromatic ring (**Figure S3**) [57]. These peaks became more prominent with increasing catechol content. The amount of DOPAC functionalization increased with increasing DOPAC added to the reaction mixture during synthesis (**Figure S4**). G-8CA microgel contained the highest amount of DOPAC content of 0.6 wt/wt% relative to the mass of the gelatin. Only 8-15% of the added DOPAC in the reaction feed was coupled to the microgel, potentially due to chemical coupling of the catechol occurred only at the surface of the microgel.

3.2. H_2O_2 Generation from Microgels

The microgels started to generate H_2O_2 once they were hydrated in PBS (**Figure 4**). The amount of generated H_2O_2 continued to increase over 24 h. The concentration of H_2O_2 generated increased with DOPAC concentration with G-8CA generating the highest amount of H_2O_2 (86 µM) after 24 h. Both G-2CA and G-4CA contain lower amounts of DOPAC and generated lower concentrations of H_2O_2 (33 and 57 µM, respectively, in 24 h). This is in agreement with the previously published data where increasing catechol content in a microgel increased the amount of H_2O_2 generation [58].

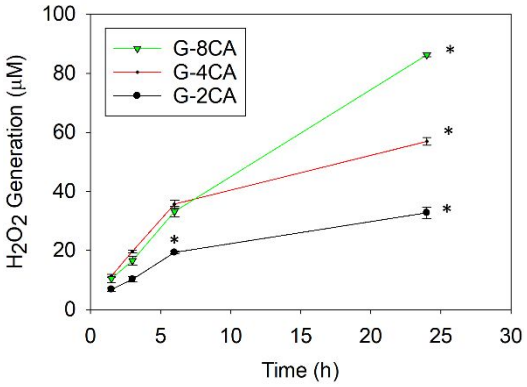

Figure 4. H_2O_2 generation from catechol containing microgels. *p < 0.001 when compared to the other microgels at the same time point.

3.3. Hydrogel Film Formation

To form hydrogel films, microgel particles were first hydrated with PBS and then lightly shaped in between two glass slides using a silicone rubber ring as a mold (**Figure S1**). Immediately after hydration, the microgels lacked cohesive property and could be easily separated from each other (**Video S1**). After the hydrated microgels were incubated for more than 30 minutes at 37°C, these microgels transformed into a hydrogel film. These films behaved like cohesive hydrogels with sufficient mechanical property to withstand tensile deformation (**Video S2**). These gelatin microgels are physically crosslinked through reversible physical interactions such as hydrogen bonds and Van der Waals forces [37]. This makes them susceptible to undergo a physical transition to form a hydrogel film when hydrated in an aqueous solution.

FESEM images further confirmed the transition of the microgels into hydrogel films (**Figure 5**). Microgels were spherical in shape with an average diameter of around 50 µm (**Table 1**). Functionalizing the gelatin microgels with DOPAC did not significantly affect the shape and size of the microgels. FESEM images of the dried hydrogel films exhibited typical network structures of hydrogels (**Figure 5B**).

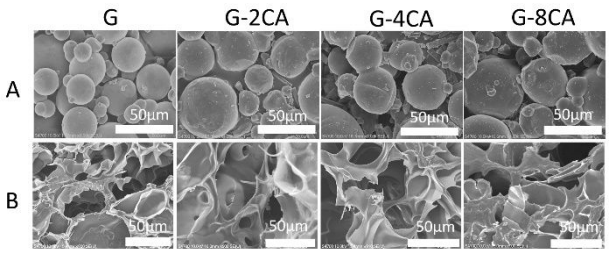

Figure 5. FESEM images of (A) microgels and (B) hydrogel films.

Table 1. Average particle size of dried microgels.

	G	G-2CA	G-4CA	G-8CA
Diameter (µm)	50.9±12	51.2±8	50.3±9	53±12

Oscillatory rheometry was performed to determine the viscoelastic property of the microgel suspensions and hydrogel films. When the microgels were initially hydrated, the storage modulus (*G'*) was always larger than the loss modulus (*G"*) throughout the linear viscoelastic regime (LVR) for all the formulations tested (**Figure 6A**). Although these microgels are discrete particles, the condensed microgel dispersion behaved like a continuous polymer network structure similar to microgel suspensions reported by others [59]. After the microgels were incubated at 37°C for 48 h, the hydrogel films did not exhibit noticeable increase in the *G'* values (**Figure 6B** and **Figure S5**). There was no change in the polymer concentration between the microgel suspensions and the hydrogel films. As such, *G'* values remained the same. However, tan δ values throughout the LVR decreased as the microgels transformed into a hydrogel film (**Figure S6** and **Table S1**). tan δ equals to *G"*/*G'* and a decrease in the tan δ value indicates that the microgels has transformed into a film that is more elastic than the microgel suspension [60]. Finally, the crossover point between the *G'* and *G"* values is often utilized to determine the yield point of a material [61]. After film formation, the *G'*-*G"* crossover point occurred at a lower strain for all formulations (**Figure S5** and **Table S1**), which further confirms the transition from discrete microgel particles to interconnected hydrogel networks over time.

Changes in catechol content did not affect the observed *G'* and *G"* values of the microgels and hydrogel films (**Figure 6**).

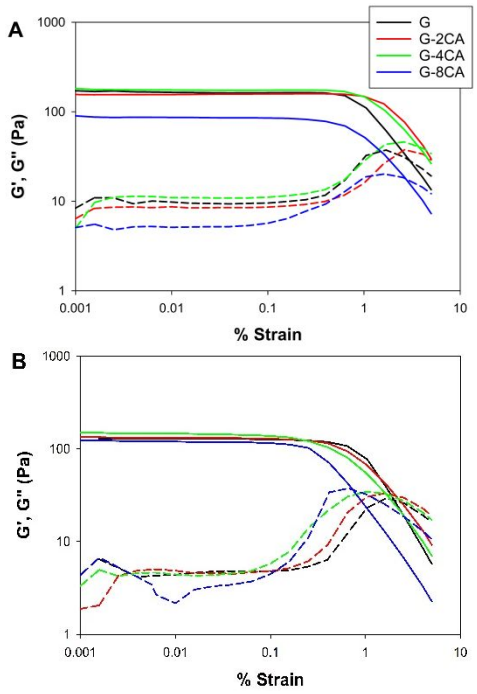

Figure 6. (A) *G'* (solid lines) and *G"* (dashed lines) for microgel suspensions examined right after hydration and (B) hydrogel films that were incubated at 37°C for 48 h.

Catechol contents in these microgels are relatively low (< 0.6 wt%) (**Figure S4**) and the observed viscoelastic property is likely contributed mostly by the physical crosslinking of gelatin, which makes up more than 99 wt% of these biomaterials. However, increasing catechol content decreased the yield strain as determined by the *G'-G"* crossover point and tan δ values (**Figure 6** and **Table S1**). These observations indicate that catechol increased the elasticity of the hydrogel films potentially through crosslink formation. Catechol is capable of forming both covalent and non-covalent (e.g., π–π and π–cation interactions, hydrogen bonding, etc.) crosslinks [62].

3.4. JKR Contact Mechanics Test

JKR contact mechanic testing was performed to evaluate the interfacial bonding properties of catechol-modified microgels to NH_2-functionalized quartz surfaces (**Figure 7**). The NH_2-functionalized quartz was used to mimic primary amine groups found on tissue surfaces [63]. Only the G-8CA hydrogel film exhibited strong adhesion to NH_2-functionalized surface with an average W_{adh} value of around 1300 mJ/m^2 (**Figure 7B**). Catechol moieties likely interact with the NH_2-functionalized surface through strong π-cation interaction and H-bonding [39]. The other formulations demonstrated weak interfacial bonding to the NH_2-functionalized surface with W_{adh} values of 70-170 mJ/m^2. The catechol content in both G-2CA and G-4CA were too low to enhance their adhesive properties. Whereas the higher concentration of catechol incorporated into G-8CA increased the chance for the catechol moieties to be present on the surface of the hydrogel film to achieve elevated adhesion.

3.5. Antibacterial Activity

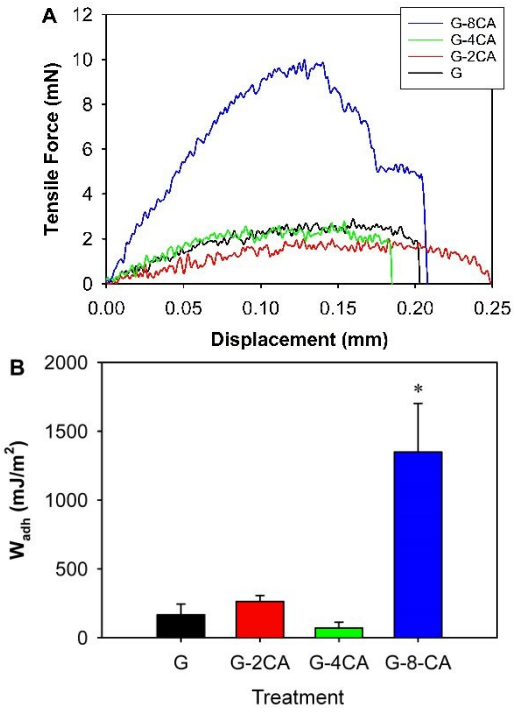

Figure 7. (A) Typical JKR contact curves and (B) work of adhesion (W_{adh}) for hydrogel films tested against a NH_2-functionalized quartz surface. *p < 0.001 when compared to other hydrogels.

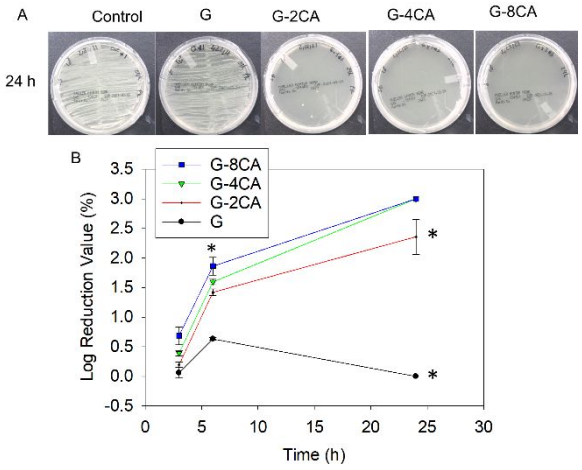

Figure 8. (A) Photographs of the test plates with *S. epidermidis* colonies after their exposure to 5 v/v% broth (control), and G, G-2CA, G-4CA, and G-8CA microgels for 24 h. (B) Log reduction values for *S. epidermidis* colonies incubated with G, G-2CA, G-4CA, and G-8CA microgels, normalized by the number of colonies formed by the bacteria exposed to 5 v/v% broth. *p < 0.05 when compared to the other microgels at the same time points.

The antibacterial properties of microgels were investigated using gram-positive *S. epidermidis* bacteria with the starting concentration of 10^3 CFU/mL (**Figures 8** and **S7**). *S. epidermidis* is a common skin colonizing bacteria and the most frequent cause of nosocomial and community-acquired skin infections [64]. Both G-4CA and G-8CA were able to achieve the highest LRV (100% reduction and LRV of 3) when incubated with *S.*

epidermidis for 24 h. G-2CA was also able to kill the bacteria and achieve 99.6% reduction (LRV = 2.3) after 24 h of incubation. The bacteria exposed to the catechol-free G microgels rapidly replicated over time and reached a very high concentration within 24 h. This data agrees with prior reports where formulations with higher catechol contents demonstrated better bactericidal effects due to their ability to generate higher amounts of H_2O_2 [25, 29].

3.6. In vitro cytotoxicity of H_2O_2-releasing microgels

The cytotoxicity of microgels was determined by directly exposing the HaCaT cells to the microgels using Resazurin cell viability assay (**Figure 9**). Microgels releasing lower amounts of H_2O_2 (G, G-2CA, and G-4CA) demonstrated cell viability of more than 80%. However, G-8CA generated the highest amount of H_2O_2 (86 µM, **Figure 4**) and exhibited a significantly lower cell viability of 74% when compared to G. This data corresponds to our previous findings, that H_2O_2 generated by catechol can reduce cell viability in culture[65]. Nevertheless, cell viability above 70% is considered noncytotoxic based on ISO 10993 standard[66].

The addition of catalase, an enzyme that decomposes H_2O_2 into water and O_2 improved cell viability to over 90% for catechol-containing samples (**Figure 9**). For G-8CA specifically, the addition of catalase increased cell viability from 74% to 94%. This result indicates that the lower cell viability observed for G-8CA can be attributed to the higher concentration of H_2O_2 released from the microgel. A simple cell culture medium lacks antioxidant enzymes naturally present in the body such as catalase, glutathione peroxidase, and peroxiredoxin, which are capable of decomposing H_2O_2 [7, 47].

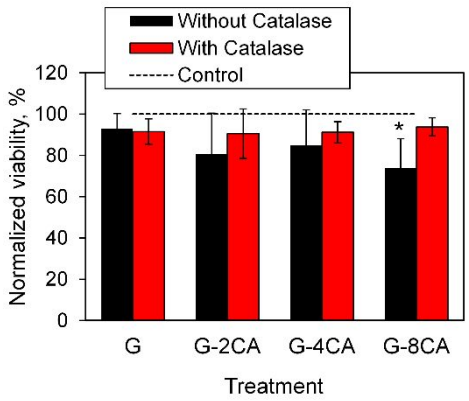

Figure 9. Cell viability of HaCaT directly exposed to G, G-2CA, G-4CA, and G-8CA in the absence (black) and in the presence (red) of catalase (2000-5000 U/ml). Untreated cells cultured on polystyrene (PS) are used as control. The results are normalized relative to PS. *$p < 0.05$ when compared to G.

3.7. VEGF level expressed by HaCaT cells in response to H_2O_2-releasing microgels

The quantity of VEGF in the HaCaT cells culture medium was measured by ELISA kit after 24 h of direct exposure to the microgels (**Figure 10**). In the absence of microgel, an average VEGF level of 32.0 pg/mL per 20,000 cell/cm^2 was measured after 24 h, serving as the control. Significantly higher VEGF level was expressed by cells directly exposed to G microgels (71.0. pg/mL) when compared to the control. Gelatin mimics the structural and biochemical properties of native extracellular matrix, promoting cell adhesion, proliferation, and activation of key signalling pathways, thereby inducing VEGF production and angiogenic responses [68, 69]. Additionally, the hydrophilic nature of gelatin supports cellular hydration and nutrient availability, promoting VEGF secretion. When HaCaT cells were exposed to H_2O_2-releasing microgels, a dose dependent upregulation of VEGF level was observed. VEGF content increased for microgels that generated higher amounts of H_2O_2. Particularly, G-8CA generated the highest H_2O_2 amongst the microgel formulations and exhibited the highest VEGF secretion at 81.0 pg/mL. This observation is consistent with previous findings indicating that increasing H_2O_2 concentration enhances VEGF expression in HaCaT cells, contributing to angiogenesis and wound healing [10, 67].

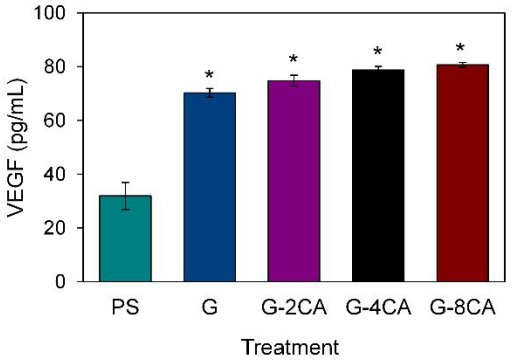

Figure 10. VEGF expression in HaCaT after 24 hours of direct exposure to G, G-2CA, G-4CA, and G-8CA microgels, compared to untreated cells cultured on polystyrene (PS) as the control. VEGF release in the culture media was quantified using ELISA. *$p < 0.05$ when compared to other samples.

3.8. Full-Thickness Dermal Wound Healing in Diabetic Mice

Full-thickness dermal wounds in healing-impaired diabetic mice were treated with catechol-modified microgels. The genetically diabetic mice model is one of the most suitable models for studying delayed wound healing [31]. Wound closure in diabetic mice is delayed by 7-10 days, regardless of the wound size, when compared to that of healthy mice. G-2CA and G-8CA were chosen as these formulations generated the lowest and highest concentrations of H_2O_2, respectively, among the catechol-modified microgels (33 and 86 µM over 24 h, respectively). These formulations will provide information regarding the effect of H_2O_2 concentration on wound healing. Catechol-free G was chosen as one of the controls. G does not release H_2O_2 and will be utilized to determine the effect of gelatin on wound healing. These microgel-treated wounds were compared with untreated open wounds (OP).

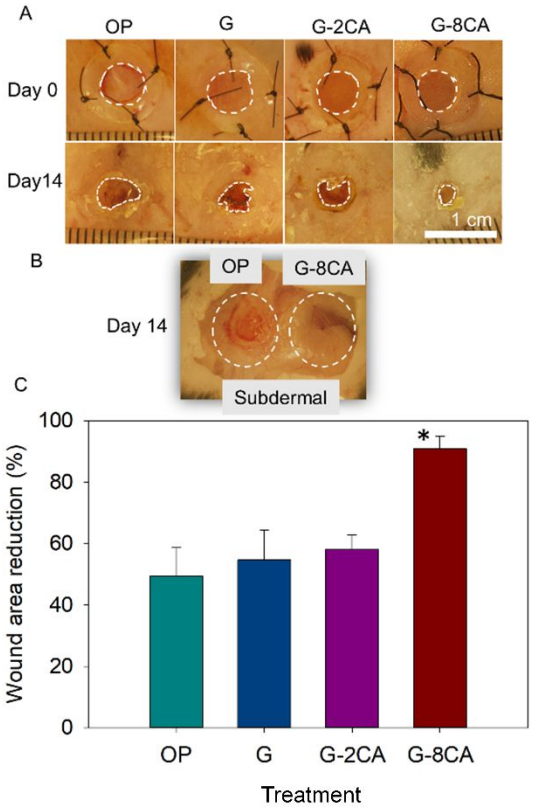

Figure 11. (A) Representative images of the wounds were taken on days 0 and 14. The white dashed lines trace the outer edge of the wound. (B) Photograph of the subdermal region and scar formation for OP and G-8CA treatments on day 14. (C) Percent wound reduction at day 14 post surgery. *p < 0.001 when compared to other treatments.

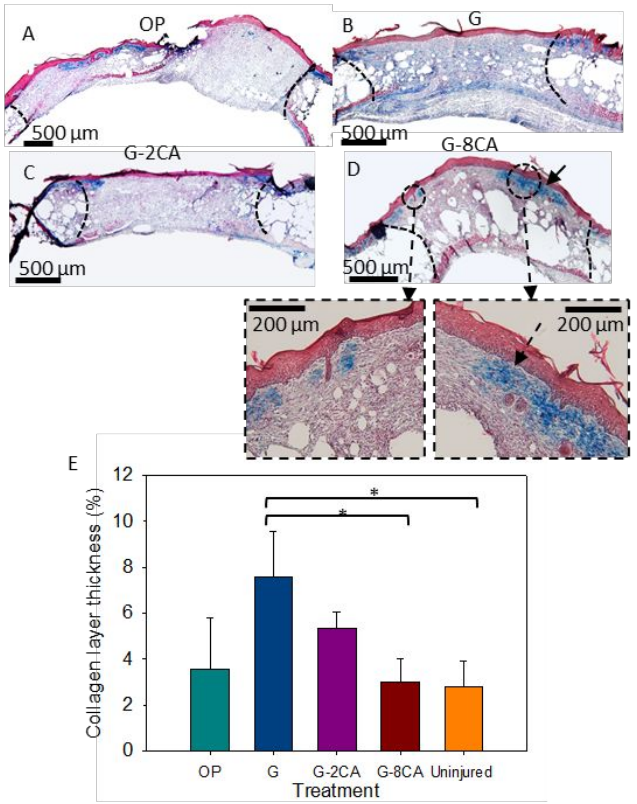

Figure 12. Representative trichrome staining of (A) OP and wound treated with (B) G, (C) G-2CA, and (D) G-8CA at day-14 post surgery. Higher magnification images show the encircled areas containing the regenerated hair follicle (left) and remodelled collagen (right; black arrow). (E) Collagen layer thickness of the treated and OP as measured in a 1 mm × 1 mm area at the wound bed. The black dashed line represents the wound margins. *p < 0.05.

At day 14, only the wounds treated with G-8CA exhibited a significant reduction in wound size (90% reduction) when compared with OP (**Figure 11**). The wounds treated with G and G-2CA only reduced the wound size by around 55%, which were not significantly different from that of OP (49%). This indicated that the higher amount of H_2O_2 released from G-8CA significantly enhanced the rate of wound closure. Additionally, Masson's Trichrome staining indicated that only G-8CA-treated wounds demonstrated a complete re-epithelialization, PC muscle formation, and appearance of hair follicles (**Figure 12**). Notably, the growth of the hair follicles (black dashed circles in **Figure 12D**) as early as 14 days post-surgery was considered as a sign of rapid wound healing in a diabetic wound model [52]. Additionally, granulation tissue and deposited collagen receded to the fibroblast-rich dermis (FD) layer, which is consistent with the morphology and structure found in native tissue. The collagen layer thickness for G-8CA-treated wounds was determined to be around 3% which agrees with that of the uninjured tissue of 2.8% (**Figure 12E**). This indicated that the G-8CA-treated wounds were at the late stages of wound healing. These results are consistent with the data reported for the 8-mm diabetic wounds treated with a transcription factor after 42 days of wounding [70].

Both G- and G-2CA-treated wounds exhibited incomplete re-epithelization and a higher amount of granulation tissue formation and collagen layer thickness (7.5 and 5%, respectively) within the wound bed when compared with that of OP (3.6%). This is consistent with an early stage of wound healing where a higher concentration of granulation tissue formation leads to connective tissue formation, prior to the healing of the injured tissue [52 70]. OP exhibited delayed wound healing with patchy granulation tissue formation and low collagen deposition when compared with the treated wounds. No hair follicle was observed within the wounds treated with G- and G-2CA microgels and the OP. These results indicated that gelatin alone and a lower amount of H_2O_2 release from G-2CA microgel do not accelerate wound healing to the extent of G-8CA-treated wounds.

K-6 staining was used to evaluate keratinocyte recruitment to the wound bed (**Figure 13**). G- and G-2CA-treated wounds exhibited the highest K-6 positive cells ratio (5.5 and 7.5%, respectively) when compared to OP (2%). Keratinocyte differentiation and migration to the wound bed are critical for efficient re-epithelialization and wound healing [71]. The OP showed the lowest K-6 positive cells ratio, which resulted in

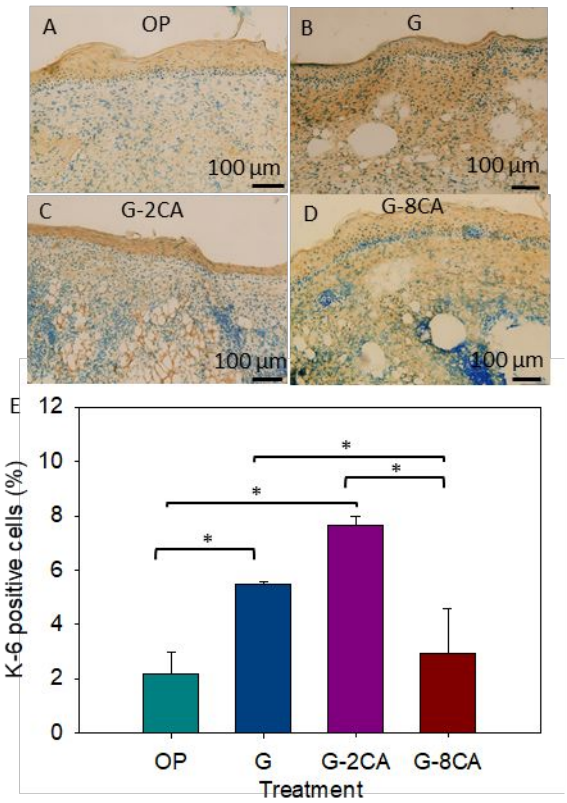

Figure 13. Representative K-6 staining of (A) OP and wound treated with (B) G, (C) G-2CA, and (D) G-8CA at day-14 post surgery. (E) Percentage of K-6 positive cells at the wound site as measured from a 1 mm × 1 mm area. K-6 positive cells are stained brown, and blue indicates the nuclei and provides overall tissue contrast. *p < 0.05.

incomplete re-epithelialization and delayed wound healing. G-8CA-treated wounds also exhibited low keratinocyte content (3%). While both OP and G-8CA-treated wounds exhibited low levels of keratinocyte recruitment, the implications differ significantly. In OP wounds, the low K-6 positive cell ratio is indicative of a prolonged inflammatory phase and failure to recruit sufficient keratinocytes necessary for re-epithelialization, leading to incomplete wound closure and delayed healing. Conversely, the low keratinocyte content in G-8CA-treated wounds indicates early maturation of keratinocytes. This is characterized by their transition from a proliferative phase to a differentiation state, which is crucial for the remodelling phase of wound healing [72]. This process involves the formation of a stable epidermal barrier and is associated with the regulation of dermal fibroblast activity, promoting rapid and efficient dermal wound healing. Therefore, while both treatments result in lower keratinocyte levels at day 14, the context and outcomes differ, with G-8CA promoting a more advanced stage of wound maturation and remodelling compared to the stalled healing observed in OP wounds.

Staining of CD68-positive cells was performed at 2 different time points (**Figure 14**). At day 7, G-8CA recruited the highest number of macrophages (18%) to the wound site when compared to other treatments (<10%). H_2O_2 released from catechol-containing biomaterials were reported to stimulate the recruitment of the inflammatory cells to the wound bed in the early days of the implantation [22, 73]. Additionally, H_2O_2 also reportedly activates M2 macrophages differentiation, which promotes angiogenesis and tissue regeneration [9, 11]. CD68 does not distinguish between the phenotype of macrophage and additional work may be required to determine if the more regenerative M2 macrophage are found at the wound site. By day 14, G-8CA-treated wounds exhibiting the lowest number of macrophages (10%) when compared with other treatments and OP. Similarly, both G and G-2CA exhibited lower amounts of macrophages at the wound site when compared to OP. This indicates that gelatin and the release of H_2O_2 reduced the inflammatory response at the wound site. The untreated wound (OP) yielded the highest percentage of macrophages at day 14 indicating a prolonged inflammatory response and delayed wound healing, which is expected in chronic wounds or ulcers, such as typical diabetic wounds, that often exhibit prolonged inflammation and poor healing [74].

The combination of the trichrome, K-6, and CD68 staining indicated the concentration-dependent response of dermal wound healing to H_2O_2 as expected based on published data [75, 76]. The lower amount of H_2O_2 released from G-2CA (33 µM) did not significantly accelerate wound healing when compared with catechol-free G microgels. On the other hand, G-8CA microgels released a higher amount of H_2O_2, which resulted in rapid dermal wound repair and remodelling, where the healed tissue resembled the structure and morphology of the native diabetic skin tissues. G-8CA released around 86 µM of H_2O_2, which is consistent with previous findings where similar levels of H_2O_2 are desirable for promoting wound healing [16, 30, 77, 78]. The released ROS recruited inflammatory cells to the wound site and facilitated healing by promoting re-epithelialization, angiogenesis, and tissue repair [79-81].

Taken together, gelatin microgels were successfully functionalized with various amounts of DOPAC to create catechol-functionalized microgels. These microgel particles are physically crosslinked, which enable these materials to undergo physical transformation from spherical particles to hydrogel networks. This ability can be utilized for delivering the microgel particles as powder directly to the wound, which would subsequently transform into wound-covering adhesive films when hydrated. Unlike other catechol-containing adhesives and sealants [82, 83], these microgels do not require reconstitution or adding an oxidant to initiate curing of adhesive. However, the transformation from microgels to hydrogel film took over 30 min. Additional work is required to accelerate the rate of transition.

The microgels reported here are composed mainly of gelatin (>99 wt%) with catechol consisting at most 0.6 wt% in the biomaterial. Additionally, the microgel formulations tested in the dibetic dermal wound model (G, G-2CA, and G-8CA) were nearly identical in terms

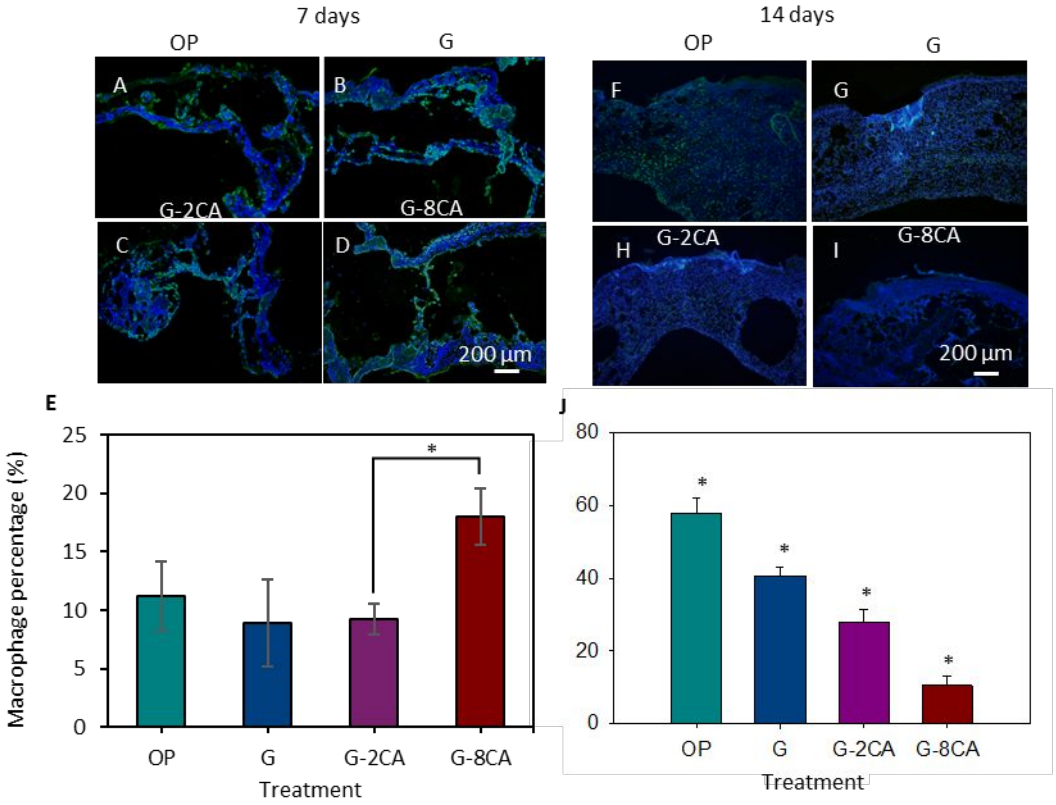

Figure 14. CD68 staining of macrophages in (A, F) OP and wounds treated with (B, G) G, (C, H) G-2CA, and (D, I) G-8CA at (A-D) 7 and (F-I) 14 days post-surgery. Cell nuclei and macrophages were stained by DAPI (blue) and CD68 (green), respectively. The percentage of macrophages relative to the total number of cells stained with DAPI after (E) 7 and (J) 14 days post-surgery. *$p < 0.05$ when compared to other treatments.

of their compositions, and mechanical and physical properties. The main difference is in the concentration of H_2O_2 generated by each formulation (0-86 µM), which remarkly contributed to the different wound healing outcomes. This result highlights the critical role of H_2O_2 in accelerating wound healing and the concentration dependent biological response to H_2O_2.

Many existing wound healing biomaterials focus on delivering growth factors, cells, peptides or other biomolecules to accelerate wound healing [84-88]. To prevent infection, silver or antibiotics are further incorporated to impart these biomaterials with antimicrobial properties [89, 90]. These approaches often involve complex formulation and high costs, limiting their scalability and application. In contrast, our microgels consist of only two ingredients: catechol and gelatin. H_2O_2 is generated in-situ as a byproduct of catechol autoxidation that can be tailored to promote dermal wound healing and wound disinfection. H_2O_2 activates many signalling pathways that promote angiogenesis and tissue regeneration [91, 92]. Moreover, the H_2O_2 released from the microgels significantly induced VEGF secretion in human keratinocytes in-vitro, demonstrating its capacity to promote wound healing. This is potentially a more cost-effective approach in creating a multifunctional biomaterial for wound healing applications.

The continuous release of H_2O_2 from our microgel demonstrated significant healing benefits, achieving comparable results with other reported biomaterials. While the therapeutic efficacy of these microgels could be further enhanced by incorporating growth factors or other bioactive molecules into their structure, this study focused on evaluating the continuous release of H_2O_2 and its effectiveness in improving impaired wound healing. Future work can explore the feasibility of incorporating additional bioactive agents and investigate the adaptability of our microgel structure without compromising its scalability. Gelatin contains funtional groups (e.g., -NH_2 or -COOH) that could chemically attach biomolecules and the microgel can potentially serve as a depot for sequastering these therapeutic agents. Finally, these microgels do not contain a reservoir for storing H_2O_2. H_2O_2 is only generated as catechol was oxidized by the molecular oxygen found in the hydrating aqueous solution. This on-demand release of H_2O_2 greatly reduces the hazards associated with the storage and transportation of ROS.

Conclusions

Catechol-functionalized gelatin microgels were prepared. Upon hydration, these physically crosslinked microgel transitioned into hydrogel films. This transition was verified based on the changes in their morphology and their viscoelastic properties as determined by SEM imaging and rheological measurements, respectively. Additionally, hydration of microgels resulted in the

generation of micromolar ranges of H_2O_2 as a result of catechol autoxidation. The concentration of H_2O_2 increased with increasing catechol content. The generated H_2O_2 was antimicrobial against *S. epidermidis* and accelerated wound healing in diabetic mice. Particularly, G-8CA treatment accelerated re-epithelialization, wound closure and maturation in the full-thickness dermal wounds of healing-impaired mouse.

Conflicts of Interest

There are no conflicts to declare.

Data Availability Statement

The data supporting this article has been included as part of the Supplementary Information.

Acknowledgements

This project was supported by the National Institutes of Health under Award Nos. R15GM135875 (B.P.L) and R15GM112082 (R.M.R.), the Office of Naval Research under Award No. N00014-20-1-2230 (B.P.L.), the National Science Foundation under Award Nos. DMR 2001076 (B.P.L.) and CMMI 2119019 (B.P.L.). P.K.F. was supported by the Doctoral Finishing Fellowship provided by Michigan Technological University. F. R. was supported by the DeVlieg Foundation Fellowship. A.T. was supported by the King-Chávez-Parks Future Faculty Fellowship. We thank the Applied Chemical & Morphological Analysis Laboratory (ACMAL) at Michigan Technological University for the use of instruments and staff assistance. Electron Microscopy facility is supported by NSF MRI 1429232.

References

1. I. Federation, *Brussels, Belgium: International Diabetes Federation*, 2017.
2. G. H. Skrepnek, J. L. Mills Sr and D. G. Armstrong, *PLoS One*, 2015, **10**, e0134914.
3. R. S. Kirsner, R. Warriner, M. Michela, L. Stasik and K. Freeman, *Archives of dermatology*, 2010, **146**, 857-862.
4. D. G. Armstrong, A. J. Boulton and S. A. Bus, *New England Journal of Medicine*, 2017, **376**, 2367-2375.
5. G. L. Brown, L. B. Nanney, J. Griffen, A. B. Cramer, J. M. Yancey, L. J. Curtsinger III, L. Holtzin, G. S. Schultz, M. J. Jurkiewicz and J. B. Lynch, *New England Journal of Medicine*, 1989, **321**, 76-79.
6. A. Zografou, O. Papadopoulos, C. Tsigris, N. Kavantzas, E. Michalopoulos, T. Chatzistamatiou, A. Papassavas, C. Stavropoulou-Gioka, I. Dontas and D. Perrea, *Annals of plastic surgery*, 2013, **71**, 225-232.
7. M. Schafer and S. Werner, *Pharmacological research*, 2008, **58**, 165-171.
8. S. Roy, S. Khanna, K. Nallu, T. K. Hunt and C. K. Sen, *Mol Ther*, 2006, **13**, 211-220.
9. C. K. Sen, S. Khanna, B. M. Babior, T. K. Hunt, E. C. Ellison and S. Roy, *J. Biol. Chem.*, 2002, **277**, 33284-33290.
10. N. N. Nissen, P. J. Polverini, A. E. Koch, M. V. Volin, R. L. Gamelli and L. A. DiPietro, *Am. J. Pathol.*, 1998, **152**, 1445-1452.
11. Y. Zhang, S. Choksi, K. Chen, Y. Pobezinskaya, I. Linnoila and Z.-G. Liu, *Cell Res*, 2013, **23**, 898-914.
12. K. L. Spiller, R. R. Anfang, K. J. Spiller, J. Ng, K. R. Nakazawa, J. W. Daulton and G. Vunjak-Novakovic, *Biomaterials*, 2014, **35**, 4477-4488.
13. V. Marchetti, O. Yanes, E. Aguilar, M. Wang, D. Friedlander, S. Moreno, K. Storm, M. Zhan, S. Naccache, G. Nemerow, G. Siuzdak and M. Friedlander, *Sci. Rep.*, 2011, **1**.
14. L. Kessler, P. Bilbault, F. Ortega, C. Grasso, R. Passemard, D. Stephan, M. Pinget and F. Schneider, *Diabetes care*, 2003, **26**, 2378-2382.
15. M. G. C. Baldry, *Journal of Applied Bacteriology*, 1983, **54**, 417-423.
16. A. E. K. Loo, Y. T. Wong, R. Ho, M. Wasser, T. Du, W. T. Ng and B. Halliwell, *PLoS ONE*, 2012, **7**, e49215.
17. N. Brian, H. Ahswin, N. Smart, Y. Bayon, S. Wohlert and J. A. Hunt, *European Cells and Materials*, 2012, **24**, 249-265.
18. S. Chigurupati, M. R. Mughal, E. Okun, S. Das, A. Kumar, M. McCaffery, S. Seal and M. P. Mattson, *Biomaterials*, 2013, **34**, 2194-2201.
19. Z. Li, F. Wang, S. Roy, C. K. Sen and J. Guan, *Biomacromolecules*, 2009, **10**, 3306-3316.
20. J. H. Waite, *International Journal of Adhesion and Adhesives*, 1987, **7**, 9-14.
21. L. M. McDowell, L. A. Burzio, J. H. Waite and J. Schaefer, *Journal of Biological Chemistry*, 1999, **274**, 20293-20295.
22. H. Meng, Y. Li, M. Faust, S. Konst and B. P. Lee, *Acta Biomaterialia*, 2015, **17**, 160-169.
23. M. Mochizuki, S.-i. Yamazaki, K. Kano and T. Ikeda, *Biochimica et Biophysica Acta (BBA)-General Subjects*, 2002, **1569**, 35-44.
24. P. Kord Forooshani and B. P. Lee, *J Polym Sci A Polym Chem*, 2017, **55**, 9-33.
25. H. Meng, P. K. Forooshani, P. U. Joshi, J. Osborne, X. Mi, C. Meingast, R. Pinnaratip, J. D. Kelley, A. Narkar, W. He, M. C. Frost, C. L. Heldt and B. P. Lee, *Acta Biomater.*, 2019, **83**, 109-118.
26. P. Kord Forooshani, E. Polega, K. Thomson, M. S. A. Bhuiyan, R. Pinnaratip, M. Trought, C. Kendrick, Y. Gao, K. A. Perrine, L. Pan and B. P. Lee, *Frontiers in Chemistry*, 2019, **7**.
27. P. Kord Forooshani, R. Pinnaratip, E. Polega, A. G. Tyo, E. Pearson, B. Liu, T.-O. Folayan, L. Pan, R. M. Rajachar, C. L. Heldt and B. P. Lee, *Chemistry of Materials*, 2020, **32**, 8182-8194.
28. Z. Zhang, X. He, C. Zhou, M. Reaume, M. Wu, B. Liu and B. P. Lee, *ACS Appl. Mater. Interfaces*, 2020, **12**, 21210-21220.
29. F. Razaviamri, S. Singh, J. Manuel, Z. Zhang, L. M. Manchester, C. L. Heldt and B. P. Lee, *ACS Appl. Mater. Interfaces*, 2024, **16**, 26998–27010.
30. R. Pinnaratip, Z. Zhang, A. Smies, P. K. Forooshani, X. Tang, R. M. Rajachar and B. P. Lee, *Polymers*, 2023, **15**, 1905.
31. S. S. Scherer, G. Pietramaggiori, J. C. Mathews, R. Chan, P. Fiorina and D. P. Orgill, *Wounds: a compendium of clinical research and practice*, 2008, **20**, 18-28.
32. Q. Xing, K. Yates, C. Vogt, Z. Qian, M. C. Frost and F. Zhao, *Scientific reports*, 2014, **4**, 1-10.
33. S. S. Silva, J. F. Mano and R. L. Reis, *Critical reviews in biotechnology*, 2010, **30**, 200-221.

34. S. Huang and X. Fu, *Journal of Controlled Release*, 2010, **142**, 149-159.
35. F. Zhao, W. L. Grayson, T. Ma, B. Bunnell and W. W. Lu, *Biomaterials*, 2006, **27**, 1859-1867.
36. Y. Li, H. Meng, Y. Liu, A. Narkar and B. P. Lee, *ACS Applied Materials & Interfaces*, 2016, **8**, 11980-11989.
37. W. de Carvalho and M. Djabourov, *Rheologica Acta*, 1997, **36**, 591-609.
38. M. V. Clement, L. H. Long, J. Ramalingam and B. Halliwell, *Journal of neurochemistry*, 2002, **81**, 414-421.
39. A. R. Narkar and B. P. Lee, *Langmuir*, 2018, **34**, 9410-9417.
40. A. R. Narkar, J. D. Kelley, R. Pinnaratip and B. P. Lee, *Biomacromolecules*, 2017, **19**, 1416-1424.
41. A. Taglietti, C. R. Arciola, A. D'Agostino, G. Dacarro, L. Montanaro, D. Campoccia, L. Cucca, M. Vercellino, A. Poggi and P. Pallavicini, *Biomaterials*, 2014, **35**, 1779-1788.
42. C. M. Flanigan, A. J. Crosby and K. R. Shull, *Macromolecules*, 1999, **32**, 7251-7262.
43. H. Hertz, *Z. Reine Angew. Mathematik*, 1881, **92**, 156-171.
44. M. S. Akram Bhuiyan, J. D. Roland, B. Liu, M. Reaume, Z. Zhang, J. D. Kelley and B. P. Lee, *Journal of the American Chemical Society*, 2020, **142**, 4631-4638.
45. N. Häntzschel, R. D. Hund, H. Hund, M. Schrinner, C. Lück and A. Pich, *Macromolecular bioscience*, 2009, **9**, 444-449.
46. M.-V. Clement, L. H. Long, J. Ramalingam and B. Halliwell, *Journal of Neurochemistry*, 2002, **81**, 414-421.
47. P. Boukamp, R. T. Petrussevska, D. Breitkreutz, J. Hornung, A. Markham and N. E. Fusenig, *J Cell Biol*, 1988, **106**, 761-771.
48. J. L. Chen, T. W. J. Steele and D. C. Stuckey, *Biotechnol Bioeng*, 2018, **115**, 351-358.
49. R. D. Galiano, V. Michaels, Joseph, M. Dobryansky, J. P. Levine, G. C. J. W. r. Gurtner and regeneration, 2004, **12**, 485-492.
50. X. Wang, J. Ge, E. E. Tredget and Y. J. N. p. Wu, 2013, **8**, 302-309.
51. D. R. Griffin, W. M. Weaver, P. O. Scumpia, D. Di Carlo and T. J. N. m. Segura, 2015, **14**, 737-744.
52. N. C. Carrejo, A. N. Moore, T. L. Lopez Silva, D. G. Leach, I. C. Li, D. R. Walker and J. D. Hartgerink, *ACS Biomaterials Science & Engineering*, 2018, **4**, 1386-1396.
53. S. A. Park, L. B. C. Teixeira, V. K. Raghunathan, J. Covert, R. R. Dubielzig, R. R. Isseroff, M. Schurr, N. L. Abbott, J. McAnulty and C. J. Murphy, *Wound Repair and Regeneration*, 2014, **22**, 368-380.
54. R. Pinnaratip, H. Meng, R. M. Rajachar and B. P. Lee, *Biomedical Materials*, 2018, **13**, 025003.
55. N. S. Tan and W. J. C. p. i. m. b. Wahli, 2013, **3**, 171-185.
56. V. Baecker, 2012.
57. N. Aktaş, N. Şahiner, Ö. Kantoğlu, B. Salih and A. Tanyolaç, *Journal of Polymers and the Environment*, 2003, **11**, 123-128.
58. H. Meng, P. K. Forooshani, P. U. Joshi, J. Osborne, X. Mi, C. Meingast, R. Pinnaratip, J. Kelley, A. Narkar, W. He, M. C. Frost, C. L. Heldt and B. P. Lee, *Acta Biomaterialia*, 2019, **83**, 109-118.
59. I. Kaneda and A. Sogabe, *Colloids and Surfaces A: Physicochemical and Engineering Aspects*, 2005, **270-271**, 163-170.
60. S. Adams, W. J. Frith and J. R. Stokes, *Journal of Rheology*, 2004, **48**, 1195-1213.
61. W. Y. Shih, W.-H. Shih and I. A. Aksay, *Journal of the American Ceramic Society*, 1999, **82**, 616-624.
62. P. K. Forooshani and B. P. Lee, *J. Polym. Sci., Part A: Polym. Chem.*, 2017, **55**, 9-33.
63. N. K. Kaushik, N. Kaushik, S. Pardeshi, J. G. Sharma, S. H. Lee and E. H. Choi, *Marine drugs*, 2015, **13**, 6792-6817.
64. M. Otto, *Expert Rev Dermatol*, 2010, **5**, 183-195.
65. P. Kord Forooshani, E. Polega, K. Thomson, M. S. A. Bhuiyan, R. Pinnaratip, M. Trought, C. Kendrick, Y. Gao, K. A. Perrine, L. Pan and B. P. Lee, *Front Chem*, 2019, **7**, 631.
66. H. Kaňďárová and P. Pôbiš, *Front Toxicol*, 2023, **5**, 1337468.
67. C. K. Sen, S. Khanna, B. M. Babior, T. K. Hunt, E. C. Ellison and S. Roy, *Journal of Biological Chemistry*, 2002, **277**, 33284-33290.
68. A. Gaspar-Pintiliescu, A. M. Stanciuc and O. Craciunescu, *Int J Biol Macromol*, 2019, **138**, 854-865.
69. S. P. Ndlovu, K. Ngece, S. Alven and B. A. Aderibigbe, *Polymers (Basel)*, 2021, **13**.
70. S. L. Hansen, C. A. Myers, A. Charboneau, D. M. Young and N. Boudreau, *Am J Pathol*, 2003, **163**, 2421-2431.
71. I. Pastar, O. Stojadinovic, N. C. Yin, H. Ramirez, A. G. Nusbaum, A. Sawaya, S. B. Patel, L. Khalid, R. R. Isseroff and M. Tomic-Canic, *Advances in wound care*, 2014, **3**, 445-464.
72. A. Stunova, L. J. C. Vistejnova and g. f. reviews, 2018, **39**, 137-150.
73. H. Meng, Y. Liu and B. P. Lee, *Acta Biomaterialia*, 2017, **48**, 144-156.
74. V. Falanga, *The Lancet*, 2005, **366**, 1736-1743.
75. A. Klein-Szanto and T. J. J. o. I. D. Slaga, 1982, **79**, 30-34.
76. A. E. K. Loo, B. J. B. Halliwell and b. r. communications, 2012, **423**, 253-258.
77. V. Grotheer, M. Goergens, P. C. Fuchs, S. Dunda, N. Pallua, J. Windolf and C. V. Suschek, *Biomaterials*, 2013, **34**, 7314-7327.
78. A. E. K. Loo, R. Ho and B. Halliwell, *Free Radical Bio Med*, 2011, **51**, 884-892.
79. K. Khorsandi, R. Hosseinzadeh, H. Esfahani, K. Zandsalimi, F. K. Shahidi and H. Abrahamse, *Inflammation and Regeneration*, 2022, **42**, 40.
80. N. I. M. Fadilah, S. J. Phang, N. Kamaruzaman, A. Salleh, M. Zawani, A. Sanyal, M. Maarof and M. B. Fauzi, *Antioxidants*, 2023, **12**, 787.
81. E. A. Veal, A. M. Day and B. A. Morgan, *Molecular Cell*, 2007, **26**, 1-14.
82. C. Zhang, B. Wu, Y. Zhou, F. Zhou, W. Liu and Z. Wang, *Chem Soc Rev*, 2020, **49**, 3605-3637.
83. W. Zhang, R. Wang, Z. Sun, X. Zhu, Q. Zhao, T. Zhang, A. Cholewinski, F. Yang, B. Zhao, R. Pinnaratip, P. K. Forooshani and B. P. Lee, *Chem Soc Rev*, 2020, **49**, 433-464.
84. S. Chen, J. Shi, M. Zhang, Y. Chen, X. Wang, L. Zhang, Z. Tian, Y. Yan, Q. Li and W. Zhong, *Scientific reports*, 2015, **5**, 1-12.
85. B. Senturk, B. M. Demircan, A. D. Ozkan, S. Tohumeken, T. Delibasi, M. O. Guler and A. B. Tekinay, *Biomaterials science*, 2017, **5**, 1293-1303.
86. K. Obara, M. Ishihara, T. Ishizuka, M. Fujita, Y. Ozeki, T. Maehara, Y. Saito, H. Yura, T. Matsui and H. Hattori, *Biomaterials*, 2003, **24**, 3437-3444.
87. B. Lu, X. Han, D. Zou, X. Luo, L. Liu, J. Wang, M. F. Maitz, P. Yang, N. Huang and A. Zhao, *Materials Today Bio*, 2022, **16**, 100392.
88. C. Huang, W. Yuan, J. Chen, L.-P. Wu and T. You, *Molecules*, 2023, **28**, 1110.

89. A. Miron, C. Giurcaneanu, M. M. Mihai, C. Beiu, V. M. Voiculescu, M. N. Popescu, E. Soare and L. G. Popa, *Pharmaceutics*, 2023, **15**, 1606.
90. X. Deng, M. Gould and M. A. Ali, *J. Biomed. Mater. Res. B*, 2022, **110**, 2542-2573.
91. H. J. Forman, *Free Radical Biology and Medicine*, 2007, **42**, 926-932.
92. J. R. Stone and S. Yang, *Antioxidants and redox signaling*, 2006, **8**, 243-270.

Data Availability Statement

The data supporting this article has been included as part of the Supplementary Information.